Accessible dynamic micropatterns in monolayer cultures via modified desktop xurography

Raymond Tran[1], Corinne A. Hoesli[1,2]*, Christopher Moraes[1,2,3]*

[1] Department of Chemical Engineering, McGill University, 3610 rue University, Montreal, QC, Canada
[2] Department of Biomedical Engineering, McGill University, 3775 rue University, Montreal, QC, Canada
[3] Rosalind and Morris Goodman Cancer Research Center, McGill University, Montreal, QC, Canada

* co-corresponding authors

E-mail: chris.moraes@mcgill.ca ; corinne.hoesli@mcgill.ca

Keywords: wound healing assay, scratch assay, epithelial monolayer, micropatterning

Abstract

Micropatterned cell cultures provide an important tool to understand dynamic biological processes, but often require specialized equipment and expertise. Here we present subtractive bioscribing (SuBscribe), a readily accessible and inexpensive technique to generate dynamic micropatterns in biomaterial monolayers on-the-fly. We first describe our modifications to a commercially available desktop xurographer and demonstrate the utility and limits of this system in creating micropatterned cultures by mechanically scribing patterns into a brittle, non-adhesive biomaterial layer. Patterns are sufficiently small to influence cell morphology and orientation and can be extended to pattern large areas with complex reproducible shapes. We also demonstrate the use of this system as a dynamic patterning tool for cocultures. Finally, we use this technique to explore and improve upon the well-established epithelial scratch assay, and demonstrate that robotic control of the scratching tool can be used to create custom-shaped wounds in epithelial monolayers, and that the scribing direction leaves trace remnants of matrix molecules that may significantly affect conventional implementations of this common assay.

Introduction

Cell and tissue geometry are well-established to regulate cell functions such proliferation[1], migration[2], signaling[3,4], and differentiation[5]. Hence, controlling tissue shape is an important strategy in tissue engineering and regenerative medicine, but generally accessible technologies such as additive three-dimensional (3D) bioprinting are severely limited in resolution of fabricated features[6], which limits broad experimentation with this critically important parameter. Alternatively, several studies have demonstrated that patterning cells and tissues into defined shapes on two-dimensional surfaces is effective at predicting cell behaviour in three-dimensional tissues[1,7–9]. Therefore, using such 2D techniques can be an important first step in establishing cell-geometry interactions for the custom design of novel biomaterials and tissue engineering strategies.

High resolution micropatterning technologies such as microcontact printing[10–12], patterned surface blocking [5,13,14], or laser patterning [15,16] of two-dimensional surfaces can achieve precise control of cell size, shape, and colony geometry. Unfortunately, these methods frequently require expensive specialized equipment, reagents, and technical expertise. Although some commercial alternatives now exist [17–19], customization for specific applications remains a challenge in standard wet labs. Furthermore, dynamically-adhesive patterns[20,21] can provide insight into developmental and homeostatic mechanisms such as wound closure[21–23] . To resolve these issues and broadly improve accessibility to customized 2D patterning technologies, here we develop a versatile, inexpensive, and easy-to-use technique, that can create dynamic geometric cues on 2D patterned surfaces, for broad deployment in standard wet labs.

Our strategy, termed subtractive bioscribing (SuBscribe), is based on patterned removal of cells or biomaterials at any experimental time point. For example, a non-adhesive film can be mechanically removed prior to cell seeding; or the cells themselves can be mechanically removed during culture. While similar in concept to UV-based photodegradation patterning methods[15,24] or photothermal degradation[25], this mechanical process does not require specialized equipment, and can be applied on existing live patterned cultures without exposing them to potentially cytotoxic compounds[26] or thermal shock[25] during the process.

Ordinarily, mechanically subtractive biopatterning approaches such as the monolayer cell scratch assay [27–29], are limited in positional resolution and pattern shape[27,30,10,31,32]. Computerized robotic controls could overcome these handling limitations to precisely damage[33] or pattern tissues by improving precision, consistency, and reducing operator errors[34]. These micromanipulation technologies previously required considerable expertise and specialized equipment, but simple modifications to commercially-available and inexpensive hobby crafting tools, such as desktop craft cutters or xurographers[35–37,37,38] are easy pathways towards automation. We and others have previously used such modified tools to etch microfluidic channels in plastic[39,40], and here we modify the craft cutter to mechanically 'scratch' biomaterials and cell layers, using scribes selected to control the size of the desired patterns. In this way, we robustly produce features smaller than the positional resolution of the craft cutter over large culture areas. We demonstrate the utility of this technique to control the shape of multicellular clusters; and use this system to investigate the role of wound geometry on closure rates of established cultures.

Results

Optimization of agarose film thickness for scratch-based micropatterns

The blade of an inexpensive, electronically controlled desktop craft cutter (KNK Zing Air; ~$800) was replaced with a metal needle to precisely scratch preprogrammed shapes into the surface. Thin agarose films are cell-repellent due to their characteristically low protein adsorption and are sufficiently brittle to be mechanically patterned with high fidelity[41]. To create the initial patterns of cells, the SuBscribe system was used to physically scratch patterns into dehydrated agarose films (Figure 1A)**.** The agarose concentration and spin coating parameters were used to tune film thickness.

Thinner agarose films, (approximately 40 nm, measured via 3D laser confocal scanning microscopy; Supplementary Figure S1) yielded the best SuBscribe pattern fidelity (Figure 1B). Furthermore, scribing of the agarose film layer did not result in any observable physical damage to the underlying glass surface (Supplementary Figure S1). Thicker layers produced with a 1% agarose solution resulted in film delamination from the underlying glass substrate, likely due to poor adhesion[21]. Thicker layers were also subjected to more cracking and delamination during

scribing, as the critical delamination[42–44] is proportional to the film thickness and needle penetration depth, which resulted in poor pattern quality. We experimentally determined that such thin films could be formed by decreasing agarose content to 0.5% and spin coating at 1500 RPM; or dip-coating glass slides in a 0.25% agarose solution (Supplementary Figure S2). While dip-coating is readily accessible to all labs and can be used to create large films, it can also result in non-uniform film thickness at the glass slide edge. For these proof of concept experiments, we therefore spin-coated our films in all subsequent experiments but note that dip-coating concentrations and surface tensions can be optimized as needed to make this technique accessible without spin-coating equipment.

Characterized limits of scratch-based micropatterning

The smallest spacing between patterns allowable was ~35 μm, which was slightly above the advertised x-y resolution limits (25 μm) of the craft cutter (Figure 1B, Supplementary Figure S3A). This allowed us to increase pattern line width by strategically programming micropattern designs (Supplementary Figure S3B). The feature sizes were defined by selecting needles of different dimensions, and when scratched across a surface, the needle diameter dictates the width of the micropatterned lines (Figure 1C). Sometimes larger needles produced feature sizes smaller than expected from the needle geometry, and this could be attributed to incomplete contact between the needle and surface. The line widths created from our batch of sewing needles was 38.6 ± 5.4 μm (n = 15 needles). Micropatterns down to 10 μm wide could be produced using a microdissection needle while larger patterns could be produced with a blunt sewing needle. Due to the repetitive strikes made by our relatively malleable needles against a hard glass substrate, we wondered whether needle tip diameter would change with repeated use, thereby changing pattern dimensions with usage. Repeated load testing of the SuBscribe system with sewing needles demonstrated that some tip dulling occurred between 1000 patterns and 2000 micropatterns but was stable before and after these points (Figure 1D, E). Tip dulling was independent of pattern length or geometry (Supplementary Figure S4). Optimization of scribing tip hardness through selection of needle material could reduce the dulling effect. However, harder scribing needles that reduce tip dulling could damage the underlying glass substrate while extremely soft needles would preserve the glass substrate but may not consistently generate micropatterned surfaces. In addition,

optimization of scribing force or calibration of the needle distance to the surface can also reduce the change in line width but should be optimized for different machines (Supplementary Figure S5 and S6). These results demonstrate that this approach can consistently make well-defined and predictable patterns, suitable for high-throughput micropatterned cell culture arrays. Should even greater consistency be required, alternative scribing needles of harder materials and coatings may be used.

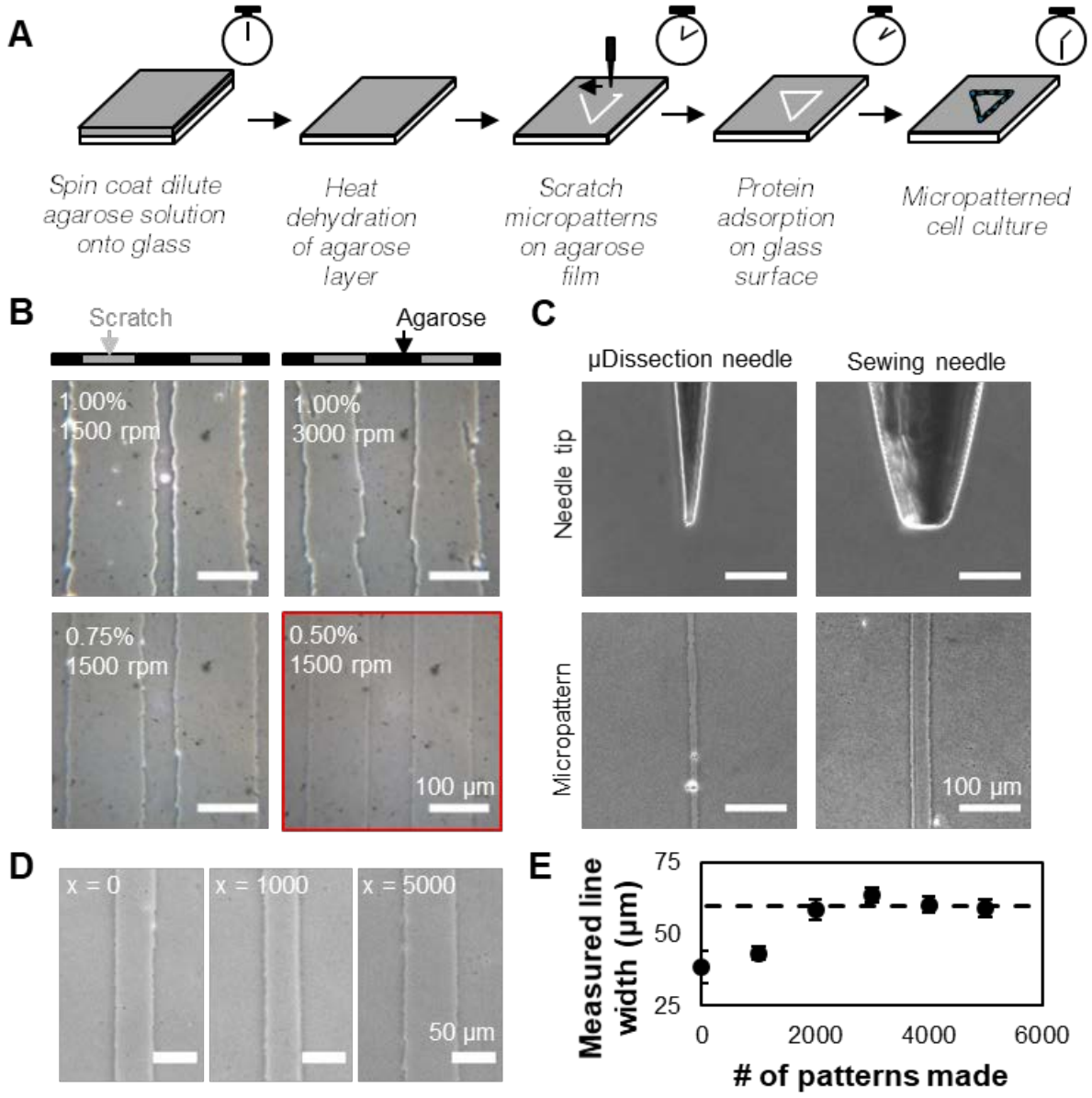

Figure 1: Production of micropatterned cell cultures via subtractive bioscribing (SuBscribing) of cell-repellant agarose layers. (A) Process flow requires less than 90 minutes to prototype slide designs. Patterns can be scribed at a speed of 2-3 mm/s allowing scribing of the patterns over a total surface area of 10 cm^2 within 10 minutes. (B) Dilute solutions of agarose reduce tearing and result in precise micropatterned substrates. Red outline denotes optimal conditions used for remaining studies. (C) Micropattern width can be varied by changing needle tip diameter. (D) Micropattern width shows insignificant degradation of a sewing needle tip over time. x represents the cumulative number of line micropatterns produced with tip. (E) Pattern width stays consistent over time. Error bars represent standard deviation over at least 15 measurements. Dashed line represents average line width after 2000 patterns scratched. Scale bars: 100 µm (B, C), 50 µm (D).

Cells confined within scratch-based micropatterns align along direction of pattern

Next, we confirmed that SuBscribed micropatterns could successfully confine cells within the desired geometries. Our patterned surfaces were first incubated with fibronectin to promote attachment in the scribed regions and seeded with human umbilical vein endothelial cells (HUVECs). Cells were confined to micropatterned lines, which limited cell attachment to the pattern widths (Figure 2). Patterns down to the width of a single cell were successfully fabricated. (Figure 2A). Furthermore, patterns made with 0.5% and 1.0% agarose solutions showed no observable difference in ability to confine cells within micropatterns (data not shown). To determine whether patterns of these dimensions were small enough to influence cell behaviour, we analysed the nuclear alignment within our scratch-based micropatterns. Confined HUVECs showed increased nuclear alignment with decreasing line width (Figure 2B), consistent with findings in HUVECs cultured on micropatterns produced with other techniques.[45] At larger pattern widths, preferential alignment direction became substantially less prominent, approaching non-patterned culture conditions. Together, these results demonstrate that cells cultured in SuBscribed micropatterns are consistent with other existing micropatterning technologies.

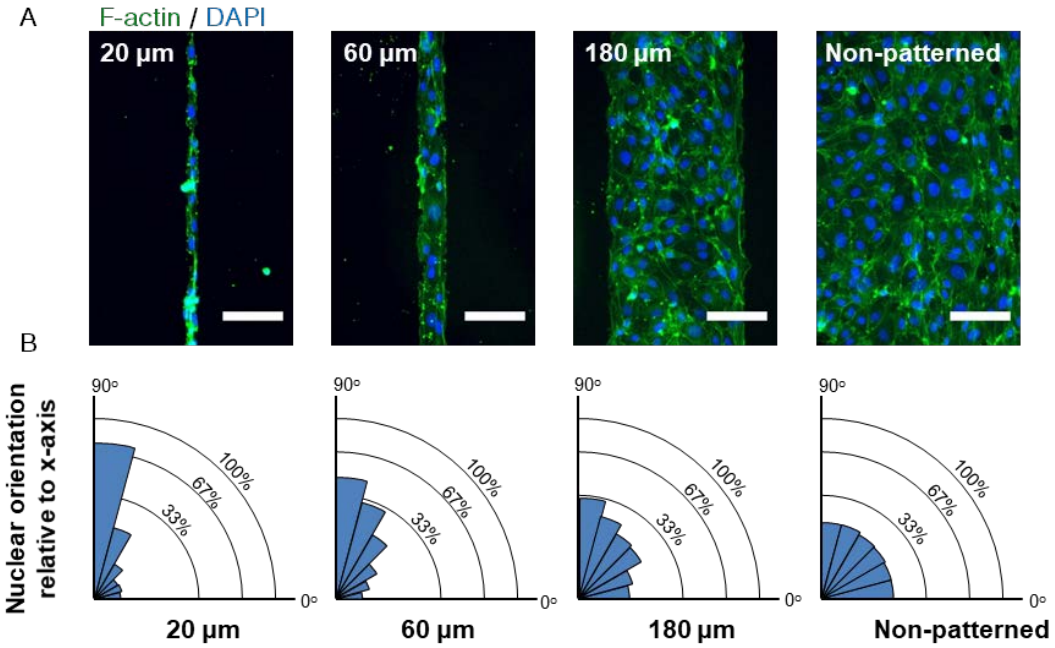

Figure 2: Scratch-based micropatterned cell cultures reproduce previously reported cell alignment. (A) Micropatterned cultures are robust and can be stained for immunofluorescent analysis. (B) Nuclei alignment correlates with decreasing line width as seen by radial histograms. Scale bars: 100 µm.

Reproducible formation of more complex micron-scale patterns

The width of the 1D patterns produced by the SuBscribe technique in the previous experiments are solely based on the needle dimensions. When creating 2D patterns, x-y "step" resolution limitations (previously shown to be ~35 µm (Supplementary Figure S2)) become more important. We therefore tested the minimum feature size limits possible when producing 2D, rounded features. The desktop craft cutter was programmed to produce circles with diameters of 2 mm down to 250 µm (Figure 3A). Circles could be fabricated reliably down to ~600 µm in diameter with less than 10% deviation from the programmed shape (Figure 3B). Smaller patterns did not retain circularity or projected size. Furthermore, small shapes were occasionally discontinuous and open, likely due to accumulated positioning errors over multiple steps. For subsequent experiments, programmed geometries were hence limited to minimum diameters of 600 µm. We confirmed that at these sizes, other basic shapes could be consistently produced while retaining sharp features (Figure 3C). We also tested our capacity to consistently pattern features over a large area with the SuBscribe technique (Figure 3D). With conventional microcontact printing approaches, multiple stamps and patterning steps would be required since it is difficult to consistently stamp a single pattern stamp over large areas, as stamps are prone to mechanical collapse and smearing of transferred proteins[46]. Patterning agarose cell-repellent surfaces using PDMS microfluidic channels directly is limited by capillary-driven flow of agarose solutions[41]. By precoating the glass substrates with the cell-repellent agarose layer, the SuBscribe system provides an alternative and less labour-intensive solution to these issues. The consistent and reproducible patterns formed 'on-the-fly' here facilitates reliable fabrication of multiple, cell-adhesive geometries over a full microscope slide (~10cm^2) in around 10 minutes, demonstrating the versatility and broad applicability of the current technique.

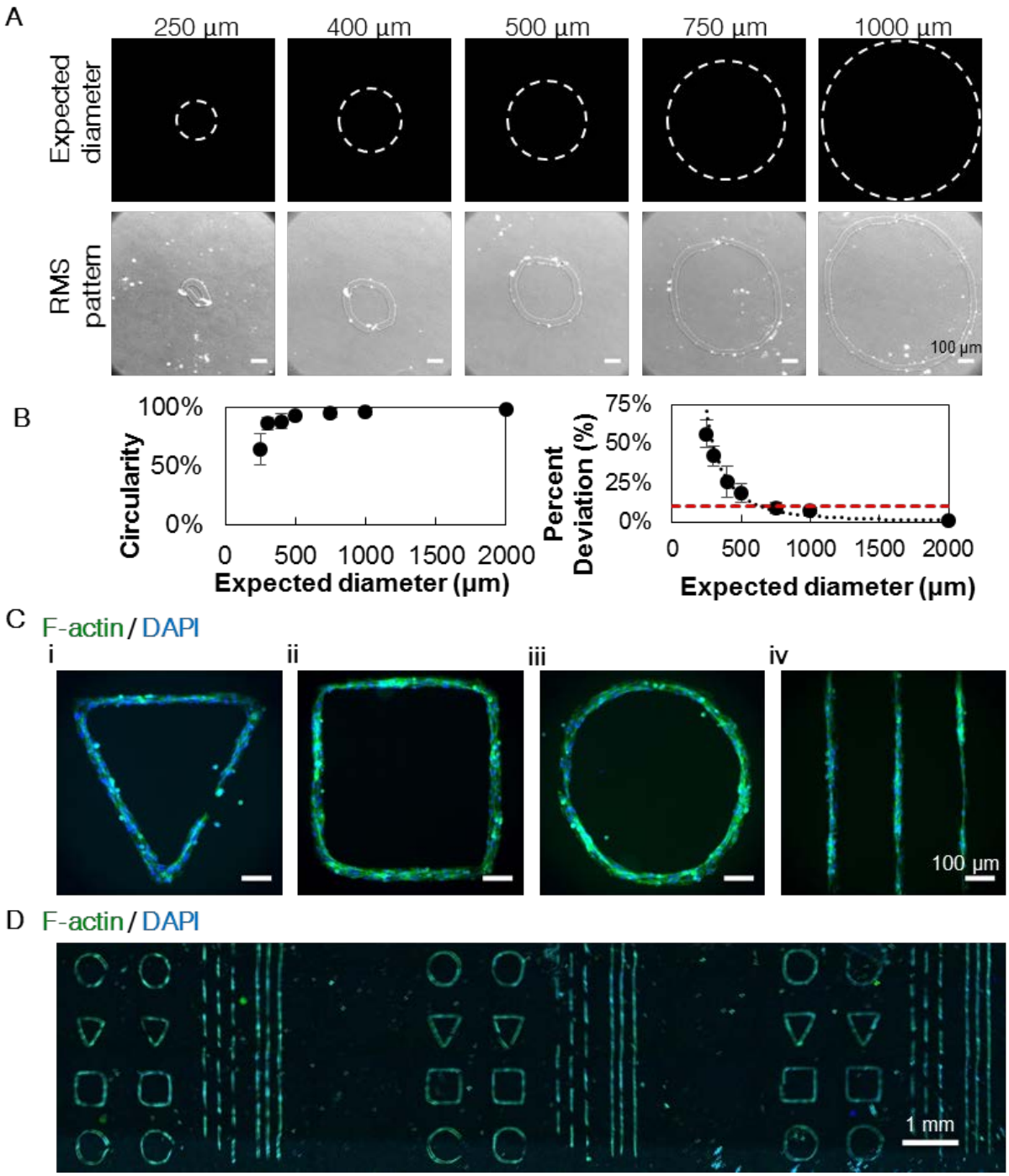

Figure 3: Scratch-based patterning technique produces consistent, micron-scale resolution patterns and allows for high-throughput screening of various geometries. (A) Annuli features can be fabricated down to 500 µm diameter with (B) high circularity and pattern fidelity. n = 20 samples were analyzed. Error bars represent standard deviation. Red dashed line represents 10% deviation from programmed patterns. (C) Magnified view of cell-laden micropatterns (i) triangle, (ii) square, (iii) circle, (iv) lines. (D) Stitched image of multiple fluorescently labelled cell micropatterns. Scale bar: 100 µm (A, C), 1 mm (D).

Dynamic modifications to agarose surface enables micropatterned co-culture

A unique feature of the SuBscribe patterning technique is that micropatterns are produced in a pre-formed non-adhesive layer, and hence requires no subsequent blocking steps that are often the cause of experimental failure in other techniques[47]. Since the entire surface is initially blocked, this technique therefore allows dynamic additions to patterns of living cultures. To demonstrate proof of principle of this concept, the SuBscribe system was used to create line-patterns, coated with fibronectin, and seeded with HUVECs (live labelled with CellTracker™ Green CMFDA) as in the previous experiment. Once cultures were established, the samples were returned to the craft cutter, and new micropatterns were formed adjacent to the living cells. After a brief incubation with fibronectin to provide attachment sites on the newly exposed glass surfaces, a 2nd population of HUVECs (live labelled with CellTracker™ Red CMTPX) were seeded on the micropatterned co-surfaces (Figure 4A). These results confirm that the co-cultured cells were well segregated between the initial and secondary micropatterns, but some cells from the second round of seeding (red) did layer themselves on top of the existing patterns of green cells. No tearing was evident in the secondary SuBscribed micropatterned lines, suggesting that hydration of the agarose film did not negatively affect pattern fidelity within the ~4 hours between initial seeding and secondary patterning.

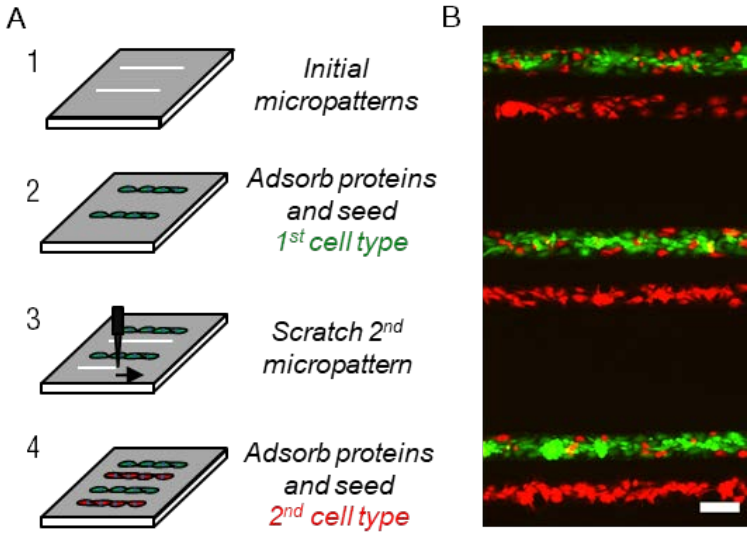

Figure 4: Technique allows for dynamic, modifiable, micropatterned cell cultures. (A) Step-by-step process to create co-cultures with multiple cell types. (B) Different HUVEC populations, stained with CellTracker™ show distinct segregation via fluorescent microscopy. Scale bar: 100 µm.

Precise, geometrically controlled wounding of live cell cultures

Since the SuBscribe technique can add new micropatterns dynamically in live cultures, scratch-based wounding can also be performed directly on a live cell monolayer. Typically, such wounding assays are performed manually with pipette tips or razor blades, with relatively poor control over wound size and shape. While specialized inserts can be custom-designed to create desired wound sizes, this requires the technological capability to produce custom devices[29,32,48], and do not recreate features of damage associated with conventional wounding strategies[49]. Typical wounds are made in a straight line, and these assays implicitly assume that the short wound edges do not contribute significantly to migration within the field of view, and that the direction of wounding does not influence closure. Using SuBscribing, a confluent monolayer of HUVEC cells cultured on a glass slide was wounded (Figure 5A, B) and closure was observed for various wound patterns and directions.

To evaluate the contributions of wound geometry towards endothelial closure time, wounds with equal areas but of varying aspect ratio (lines vs. squares) and geometry (squares vs. circles) were formed, and their closure rates were visualized over 4.5 hours with live cell imaging (Figure 5C, Supplementary Figure S5). All wounds closed over time, with wound closure velocities similar to those previously reported in *in vivo* animal studies[50]. Individual cells in wound with unity aspect ratio shapes must travel further to close, and hence we expected and confirmed that thin, line-shaped wound areas close significantly faster compared to circular and rectangular wound, with significantly faster areal closure rates in the first hour (Figure 5C, Supplementary Figure S7). These findings are consistent with delayed exponential models commonly used to describe wound closure rates[32,51,52]. In order to compare wounds of different geometry, we normalized the wound closure rate to wound perimeter[51,53,54]. This yields a linear healing parameter which represents the migration speed of the wound edge[55,56]. Line shape wounds had lower normalized migration speeds compared to square and circular geometries (Figure 5D), suggesting that thin line-shaped wounds only appear to close faster because of the aspect ratio of the wound. Tracking the cells at the wound edge also show significantly slower migration speeds in line-shaped patterns but also in circular patterns (Supplementary Figure S8) further suggesting geometric dependence of cell migration during wounding. These differences between geometries may be due to differences in migration mechanism, for example purse-string closure mechanisms[57]

versus lamellipodia-protrusion based migration[58], which may each dominate wound closure depending on local geometry.

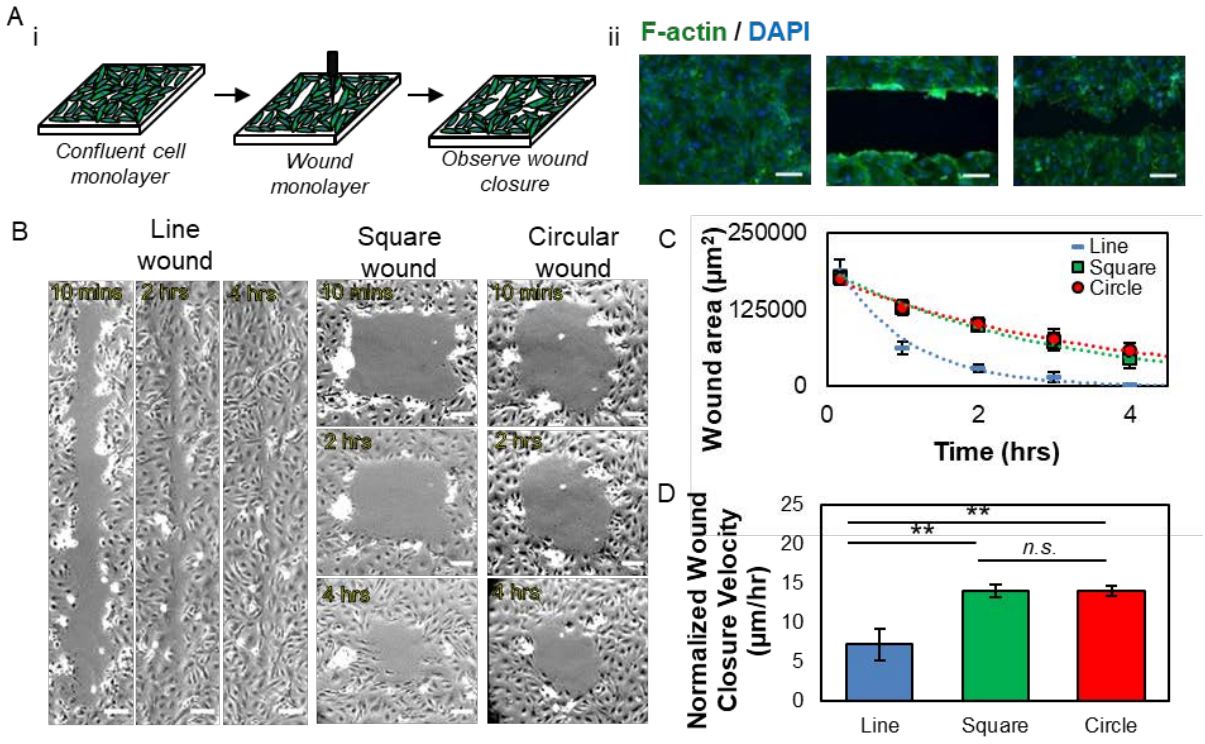

Figure 5: SuBscribe technique can be adapted to wound healing assays to test various wound lengths. (A) i) Process flow to create wounded tissues with SuBscribe. ii) Wound closure can be visualized over time with fluorescent staining. (B) Wounds with defined geometry were created using SuBscribe wounding approach and visualized over time. (C) Line-shaped wounds close fastest as shown by wound area over time. (D) Wound closure velocity normalized to wound perimeter quantified from phase contrast images during live cell imaging (n=3 for each wound type). Velocity was obtained from linear regression. * represents $p<0.05$ for a one way ANOVA with Tukey post-hoc multiple comparisons test. Scale bars: 100 μm.

A potential confounding factor in conventional scratch-based assays is the presence or absence of ECM on the denuded surface[58]. If ECM is left intact, cells can close the gap via lamellipodia-mediated adhesive migration, while ECM removal prevents lamellipodial crawling to close the wound[58,59]. In our straight-line wounds, we observe rapid migration in the first hour after wounding, accompanied by large lamellipodial extensions for cells at the leading edge. As the wound closes, these lamellipodia become smaller and fewer (Supplementary Video 1). We reasoned that the central area of the wound has greater ECM removal because of the needle profile, while the edges may retain some ECM that supports lamellipodial-assisted crawling migration. Designing needle profiles and tuning the applied loading force exerted by the craft cutter may hence provide additional control over wound quality and closure rates in subsequent studies.

We then reasoned that if remaining ECM plays a role in wound closure, then the scratching paths may leave traces of oriented ECM that guide wound closure. We are uniquely able to test this parameter by programming distinct scratching paths that wound not be possible with conventional scratching tools. To test this idea, we created a square wound using a side-to-side scratching motion (Figure 6A). We confirmed that trace nanoscale ECM cues remain in linear patterns oriented along the scratch path by staining adsorbed fibronectin on cell-free controls (Figure 6B; Supplementary Figure S8). Square-shaped wounds in cell monolayers rapidly become rectangular and closed consistently along the longitudinal scribing direction (Figure 6C, D).

We then compared the average migration velocities of HUVEC edges both parallel and perpendicular to the scratching direction (Figure 6E). The migration of cells into a circular wound, created by repeated scratching of concentric circles, was also measured and the direction of wound closure was considered perpendicular to the scratch direction. The migration velocity of HUVECs parallel to the scratch direction was significantly greater than perpendicular to the scratch direction, suggesting cues that arise from the scratching direction itself could act to guide migration. Since topographic direction of 1-D patterns of ECM is well-established to guide and enhance migration rates [16], these findings suggest an additional parameter present in conventional wound assays that may affect results, and that can be controlled for using robotically-controlled scribing assays.

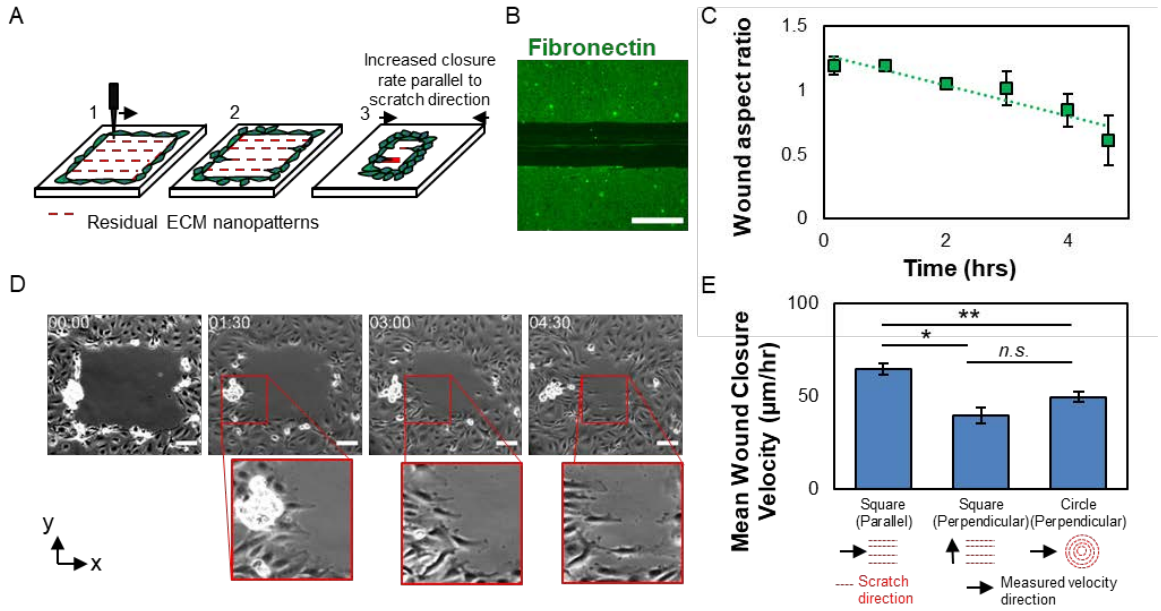

Figure 6: Nanotopographic ECM cues produced from SuBscribe technique increases migration velocity parallel to scratch direction. (A) Proposed model for increased directional migration velocity action due to remaining ECM cues after scratch patterning. (B) SuBscribe technique physically removes ECM but also leaves trails of fibronectin in direction of scribe path. (C) Asymmetric wound closure of square wounds over time results in rectangular wounds with aspect ratio < 1. (D) Representative wound closure over time in square wounds. Inset shows increased directional migration along scratch direction. Time stamps in HH:MM format. (E) Mean wound closure velocity with respect to scratch direction in different shapes. Error bars represent standard error. * represents $p<0.05$ for a one-way ANOVA with Tukey post-hoc multiple comparisons test. Scale bars: (B) 50 µm, (D) 100 µm.

Discussion

This work demonstrates a novel micropatterning strategy where thin layers of cell-repellent agarose are mechanically removed with a pointed needle, controlled by an inexpensive and readily available hobby craft cutter. Removal of agarose can produce confined cell cultures like those produced in other, more laborious micropatterning techniques. Circular micropatterns down to 600 µm can be reproducibly created in both biomaterial films and on-the-fly in live cultures, allowing subsequent patterning and seeding steps. Using this platform, we were then able to investigate the effect of precisely defined wound geometry and scribing direction on closure rate, revealing an intriguing role for nanotopographic remnant ECM in influencing wound closure rates in conventional assays. Overall, the presented SuBscribe technique provides additional consistency, throughput, capabilities and accessibility over other microengineered techniques and assays.

In this proof-of-concept work, we used a relatively inexpensive hobby craft cutter to achieve these patterns. This $800 system had an advertised positioning resolution of 25 µm, which does present some limitations on the resolution of rounded features. Micropattern resolution may be improved by hacking an inexpensive 3D printer to achieve x-y stepping resolutions down to 5 µm or using alternative vector-based craft cutters to implement the SuBscribe technique. Currently, our technique is limited in the choice of substrates; patterns cannot be generated on substrates with nanoscale features as they may be damaged during the SuBscribing process. We also limited our studies to off-the-shelf needles, which do have some limitations in available geometry and relevant material properties such as hardness. Custom-cut needles with non-standard profiles may also further improve the resolution of this technique, and the applied loading force profile may also be tuned to eliminate or retain nanotopographic ECM cues without damaging the underlying surface. Alternatively, soft silicone tips may allow further fine-tuning of these removal processes[60,61]. We also observed that different degrees of ECM cue removal can be controlled by tuning the force and calibration of the craft cutter (Supplementary Figure S10). Finally, the capacity of this technique to pattern relatively large surface areas could allow for systematic investigation of the effect of geometrically defined multicellular islands on cell function.

There may also be considerable room to expand this technique by carefully selecting alternative biomaterial films for scribing. In our experience, SuBscribe-produced agarose micropatterns could be maintained in culture for at least 3 days, but can fail after this timepoint

due to poor physical adsorption of the agarose to the underlying glass substrate[14]. Longer duration experiments would require an alternative material that is sufficiently cell-repellent and brittle and may require advanced deposition techniques to process. Our SuBscribe technique is particularly useful for prototyping new micropatterned cultures in lines or non-filled shapes with radii of curvatures greater than 600 µm. Geometries of this scale have previously been shown to drive pluripotent[62] and mesenchymal[12] stem cell differentiation, and various cell functions[5,13,63] and are important to establish soluble factor gradients within micropatterned culture. Filled-in shapes can be created by the repeated etching of concentric patterns which decrease in size, similar to the methods presented to create square or circular wounds. Increasingly complex geometries are also theoretically possible but require fine craft cutter calibration to ensure scribing errors do not propagate during patterning. With some optimization, this technique could be employed to generate numerous novel patterns to perform high-throughput screens on novel geometries. Given the demonstrated capacity of this technique to handle live cultures, we envision a dynamically tunable surface able to generate dynamic adhesive sites on demand and at selected locations, opening new avenues for investigation into responsive morphodynamic cell culture systems.

This work also builds upon conventional scratch-based wounding techniques by allowing precise control of wound geometry which has not been possible previously due to operator handling limitations[64]. Robotically-aided wounding has previously been reported but were limited to large, straight wounds[34]. Wound geometry can also be controlled using silicone-based culture inserts during cell seeding but, this approach does not allow mechanical retraction of cells on wounding, which has been shown to be important in initiating wound closure mechanisms in 2D[49] and 3D cultures[32]. Furthermore, this work demonstrates that the process of scratching may itself leave nanotopographic cues that affect observed wound closure, further emphasizing the need for an active wounding process, and precise control over wounding conditions. Interestingly, cells at the wound edge in line and circular wounds migrated slower than those in square wounds (Supplementary Figure S8). This could be due to the nanotopographic cues left from scratching, where in line and circular wounds most cells are migrating perpendicular to the wounding direction. Conversely, in square wounds ~50% of cells are migrating parallel to the wounding direction. Finally, future studies using this system could be integrated into existing platforms to investigate the role of gap closure in the a more realistic environment by better recapitulating ECM protein interactions, co-culture, or in the presence of *in vivo* flow dynamics[65].

Conclusions

Using a robotically-controlled mechanical micropatterning technique raises the possibility for dynamic micropatterning systems that would be otherwise difficult with chemical approaches. Such a system could allow for novel confined migration assays, wounding assays, or micropatterned co-cultures with greater than 2 cell types. Here, we demonstrate an approach that allows us to precisely define geometry in our wounding assay and we show the importance in considering the presence of ECM in such studies. Overall, the described SuBscribe technique provides an inexpensive, novel, and accessible route towards surface micropatterning, which will ultimately lead to improved collaborative opportunities between biomaterials scientists, engineers and fundamental biologists.

Methods

Micropatterned agarose layer preparation

A dilute stock solution of agarose in water was heated to 80 ^{o}C until completely liquid. Thin films of cell repellent agarose surfaces were fabricated by spin coating the 0.5 % UltraPure^{TM} Agarose (Invitrogen) solution at 1500 rpm for 30 seconds onto standard 25 mm x 75 mm glass slides. The slides were then placed on a hot plate set at 100 ^{o}C for 5 minutes to dehydrate the glass slide.

Microscale patterns were mechanically scratched into the dehydrated agarose film atop a glass slide using an electronically-controlled, inexpensive desktop craft cutter (KLIK-N-CUT Zing Air, KNKUSA). Sewing needles and microdissection needles were fitted into an 18-gauge needle, immobilized with epoxy, and attached to a syringe which was mounted onto the desktop craft cutter. Calibration of the z-axis was done by manually by adjusting the position of the needle holder. To ensure the cuts always contacted the substrate throughout the programmed pattern, the needle position was calibrated to cut below the glass surface (i.e. 1mm below the glass surface). Designs were created in the Make-the-Cut! software provided by the manufacturer. In this software, the cutting parameters were adjusted in the following ranges; Cutting speed: 1-10, Travel speed: 1-10, Cutting force: 50, Multi-cut: 1. The patterned substrates were coated with 25 μg/mL fibronectin (Millipore) diluted in phosphate buffered saline (PBS) for 1-2 hours and then rinsed once with PBS before cell seeding.

Cell culture

Human umbilical vein endothelial cells (HUVECs) up to passage 6 were used in RMS patterning experiments. HUVECs were cultured on 25 μg/mL fibronectin-coated tissue culture polystyrene in Medium 200 supplemented with low serum growth supplement (LSGS) (Thermo Fisher Scientific) and 1% antibiotic-antimycotic (Gibco). Medium changes were performed every 2-3 days and cells were passaged at 90% confluency. Patterned substrates were seeded with at least 50,000 cells/cm^2 to ensure confluency of patterns. Patterns were then rinsed with PBS after 2 hours to remove cells that did not adhere.

Co-culture experiments

HUVECs were fluorescently labelled with CellTracker™ Red CMTPX (Life Technologies) and CellTracker™ Green CMFDA (Life Technologies) as per manufacturer's instruction. Patterned co-culture was accomplished by sequential seeding of the two cell populations. The first cell population was treated as before, allowed 2 hours to adhere, and then rinsed once with PBS. The second patterns were immediately scribed while still in solution. Afterwards, the culture was soaked in Medium 200 supplemented with LSGS, 1% antibiotic-antimycotic, and 25 μg/mL of fibronectin to coat the new micropatterns for 1 hour. The second cell population was then seeded at 50,000 cells/cm^2, allowed 2 hours to adhere, and then rinsed of excess cells.

Immunofluorescent staining

Cell micropatterning samples were fixed with 4% paraformaldehyde for 20 minutes, washed with PBS three times, permeabilized with 0.1% Triton-X100 solution for 20 minutes, then washed with PBS three times. A cocktail of FITC-phalloidin (1:200 dilution) and the DAPI counterstain (1:1000) were diluted in PBS, incubated with the sample for 20 minutes at room temperature, then washed three times with PBS. Images were obtained on an Olympus IX73 microscope.

Fibronectin patterns were visualized with an indirect immunostaining approach. First, non-specific binding was blocked by a 30 minute incubation at room temperature with DAKO Protein Block (X0909, Agilent) and then rinsed once with PBS. The primary antibody, mouse anti-human fibronectin (SAB4200760, 1:400 dilution, Sigma) was incubated at 4 ºC overnight then washed three times with PBS. Afterwards, the corresponding secondary antibody, goat anti-mouse AlexaFluor 488 (A11001, 1:400 dilution, Life Technologies) was incubated at room temperature for 1 hour, washed three times in PBS and then visualized.

Data Analysis

All images obtained were analysed using the open-source software, Fiji[66]. The nuclear alignment of micropatterned cells was measured by approximating each nucleus as an ellipse. The angles reported represent the angle between the primary axis of the nucleus and the x-axis. Circularity of the patterns presented in Figure 3 was obtained by manually tracing the resultant micropatterns and reporting the circularity outputted by Fiji. Deviation of the micropatterns was computed as the percent difference between the expected diameter and the actual diameter of the resultant micropatterned circle. The calculated diameter was approximated with the traced perimeter of the micropatterned circle. Stitched images of the line-shaped wounds were created using the Fiji Pairwise stitching plugin[67]. Single cell tracking in Supplemental Figure S8 was performed using the MTrackJ plugin for Fiji [68]. Statistics were calculated using GraphPad Prism 8.

Acknowledgements

The authors received funding from Canada's National Sciences and Engineering Research Council (NSERC, PGS-D award for RT, RGPIN-2015-05512 to CM and RGPIN-2015-05877 to CH) which supported this work. This work was undertaken, in part, thanks to funding from the Canada Research Chairs program (CH and CM) and the 'Funding Biotechnology Partnerships' program from the Stem Cell Network. RT and CH are members of the Quebec Network for Cell, Tissue and Gene Therapy – ThéCell (a thematic network supported by the Fonds de recherche du Québec–Santé), of the Québec Center for Advanced Materials (CQMF), of PROTEO (The Quebec *Network* for Research on Protein Function, Engineering, and Applications), of the Cardiometabolic Health, Diabetes and Obesity Research Network (CMDO), and of the Montreal Diabetes Research Center (MDRC).

References

1. Nelson, C. M. *et al.* Emergent patterns of growth controlled by multicellular form and mechanics. *Proc. Natl. Acad. Sci. U. S. A.* **102**, 11594–11599 (2005).
2. Nam, K.-H. *et al.* Multiscale Cues Drive Collective Cell Migration. *Sci. Rep.* **6**, 29749 (2016).
3. Etoc, F. *et al.* A Balance between Secreted Inhibitors and Edge Sensing Controls Gastruloid Self-Organization. *Dev. Cell* **39**, 302–315 (2016).
4. Lee, W. *et al.* Dispersible hydrogel force sensors reveal patterns of solid mechanical stress in multicellular spheroid cultures. *Nat. Commun.* **10**, 144 (2019).
5. Tran, R., Moraes, C. & Hoesli, C. A. Controlled clustering enhances PDX1 and NKX6.1 expression in pancreatic endoderm cells derived from pluripotent stem cells. *Sci. Rep.* **10**, 1190 (2020).
6. Miri, A. K. *et al.* Effective bioprinting resolution in tissue model fabrication. *Lab. Chip* **19**, 2019–2037 (2019).
7. Lee, J., Abdeen, A. A., Wycislo, K. L., Fan, T. M. & Kilian, K. A. Interfacial geometry dictates cancer cell tumorigenicity. *Nat Mater* **15**, 856–862 (2016).
8. Gjorevski, N. & Nelson, C. M. Endogenous patterns of mechanical stress are required for branching morphogenesis. *Integr. Biol.* **2**, 424–434 (2010).
9. Nelson, C. M., Vanduijn, M. M., Inman, J. L., Fletcher, D. A. & Bissell, M. J. Tissue geometry determines sites of mammary branching morphogenesis in organotypic cultures. *Science* **314**, 298–300 (2006).
10. Khadpekar, A. J., Khan, M., Sose, A. & Majumder, A. Low Cost and Lithography-free Stamp fabrication for Microcontact Printing. *Sci. Rep.* **9**, 1024 (2019).
11. Chen, C. S., Mrksich, M., Huang, S., Whitesides, G. M. & Ingber, D. E. Geometric Control of Cell Life and Death. *Science* **276**, 1425 (1997).
12. Ruiz, S. A. & Chen, C. S. Emergence of Patterned Stem Cell Differentiation Within Multicellular Structures. *STEM CELLS* **26**, 2921–2927 (2008).
13. Ma, Z. *et al.* Biomimetic Micropatterned Adhesive Surfaces To Mechanobiologically Regulate Placental Trophoblast Fusion. *ACS Appl. Mater. Interfaces* **11**, 47810–47821 (2019).
14. Nelson, C. M., Raghavan, S., Tan, J. L. & Chen, C. S. Degradation of Micropatterned Surfaces by Cell-Dependent and -Independent Processes. *Langmuir* **19**, 1493–1499 (2003).
15. Vignaud, T. *et al.* Reprogramming cell shape with laser nano-patterning. *J Cell Sci* **125**, 2134–2140 (2012).
16. Doyle, A. D., Wang, F. W., Matsumoto, K. & Yamada, K. M. One-dimensional topography underlies three-dimensional fibrillar cell migration. *J. Cell Biol.* **184**, 481–490 (2009).
17. Monjaret, F. *et al.* Fully Automated One-Step Production of Functional 3D Tumor Spheroids for High-Content Screening. *J. Lab. Autom.* **21**, 268–280 (2015).
18. Young, J. *et al.* MyoScreen, a High-Throughput Phenotypic Screening Platform Enabling Muscle Drug Discovery. *SLAS Discov. Adv. Sci. Drug Discov.* **23**, 790–806 (2018).
19. Bosch-Fortea, M. *et al.* Micropattern-based platform as a physiologically relevant model to study epithelial morphogenesis and nephrotoxicity. *Biomaterials* **218**, 119339 (2019).

20. Rodriguez, N. M., Desai, R. A., Trappmann, B., Baker, B. M. & Chen, C. S. Micropatterned multicolor dynamically adhesive substrates to control cell adhesion and multicellular organization. *Langmuir ACS J. Surf. Colloids* **30**, 1327–1335 (2014).
21. Raghavan, S., Desai, R. A., Kwon, Y., Mrksich, M. & Chen, C. S. Micropatterned Dynamically Adhesive Substrates for Cell Migration. *Langmuir* **26**, 17733–17738 (2010).
22. Almeida, F. V. *et al.* High-Content Analysis of Cell Migration Dynamics within a Micropatterned Screening Platform. *Adv. Biosyst.* **3**, 1900011 (2019).
23. van Dongen, S. F. M., Maiuri, P., Marie, E., Tribet, C. & Piel, M. Triggering Cell Adhesion, Migration or Shape Change with a Dynamic Surface Coating. *Adv. Mater.* **25**, 1687–1691 (2013).
24. Strale, P.-O. *et al.* Multiprotein Printing by Light-Induced Molecular Adsorption. *Adv. Mater.* **28**, 2024–2029 (2016).
25. Moriguchi, H. & Yasuda, K. Photothermal Microneedle Etching: Improved Three-Dimensional Microfabrication Method for Agarose Gel for Topographical Control of Cultured Cell Communities. *Jpn. J. Appl. Phys.* **45**, L796–L799 (2006).
26. Brandenberg, N. & Lutolf, M. P. In Situ Patterning of Microfluidic Networks in 3D Cell-Laden Hydrogels. *Adv. Mater.* **28**, 7450–7456 (2016).
27. Liang, C.-C., Park, A. Y. & Guan, J.-L. In vitro scratch assay: a convenient and inexpensive method for analysis of cell migration in vitro. *Nat. Protoc.* **2**, 329 (2007).
28. Rodriguez, L. G., Wu, X. & Guan, J.-L. Wound-Healing Assay. in *Cell Migration: Developmental Methods and Protocols* (ed. Guan, J.-L.) 23–29 (Humana Press, 2005). doi:10.1385/1-59259-860-9:023.
29. Jonkman, J. E. N. *et al.* An introduction to the wound healing assay using live-cell microscopy. *Cell Adhes. Migr.* **8**, 440–451 (2014).
30. Javaherian, S., O'Donnell, K. A. & McGuigan, A. P. A Fast and Accessible Methodology for Micro-Patterning Cells on Standard Culture Substrates Using Parafilm™ Inserts. *PLOS ONE* **6**, e20909 (2011).
31. Wright, D. *et al.* Reusable, reversibly sealable parylene membranes for cell and protein patterning. *J. Biomed. Mater. Res. A* **85A**, 530–538 (2008).
32. Dubois, S. J., Kalashnikov, N. & Moraes, C. Robust and Precise Wounding and Analysis of Engineered Contractile Tissues. *Tissue Eng. Part C Methods* **25**, 677–686 (2019).
33. Sakar, M. S. *et al.* Cellular forces and matrix assembly coordinate fibrous tissue repair. *Nat. Commun.* **7**, 11036 (2016).
34. Simpson, K. J. *et al.* Identification of genes that regulate epithelial cell migration using an siRNA screening approach. *Nat. Cell Biol.* **10**, 1027 (2008).
35. D. A. Bartholomeusz, R. W. Boutte & J. D. Andrade. Xurography: rapid prototyping of microstructures using a cutting plotter. *J. Microelectromechanical Syst.* **14**, 1364–1374 (2005).
36. Speller, N. C. *et al.* Cutting edge microfluidics: Xurography and a microwave. *Sens. Actuators B Chem.* **291**, 250–256 (2019).
37. Stallcop, L. E. *et al.* Razor-printed sticker microdevices for cell-based applications. *Lab. Chip* **18**, 451–462 (2018).
38. Álvarez-García, Y. R. *et al.* Open multi-culture platform for simple and flexible study of multi-cell type interactions. *Lab. Chip* **18**, 3184–3195 (2018).

39. Guckenberger, D. J., de Groot, T. E., Wan, A. M. D., Beebe, D. J. & Young, E. W. K. Micromilling: a method for ultra-rapid prototyping of plastic microfluidic devices. *Lab. Chip* **15**, 2364–2378 (2015).
40. Chandrasekaran, A. *et al.* Thermal scribing to prototype plastic microfluidic devices, applied to study the formation of neutrophil extracellular traps. *Lab. Chip* **17**, 2003–2012 (2017).
41. Nelson, C. M., Liu, W. F. & Chen, C. S. Manipulation of Cell-Cell Adhesion Using Bowtie-Shaped Microwells. in *Adhesion Protein Protocols* (ed. Coutts, A. S.) 1–9 (Humana Press, 2007). doi:10.1007/978-1-59745-353-0_1.
42. Roy, S., Darque-Ceretti, E., Felder, E., Raynal, F. & Bispo, I. Experimental analysis and finite element modelling of nano-scratch test applied on 40–120nm SiCN thin films deposited on Cu/Si substrate. *Thin Solid Films* **518**, 3859–3865 (2010).
43. Kang, C.-W. & Huang, H. Deformation, failure and removal mechanisms of thin film structures in abrasive machining. *Adv. Manuf.* **5**, 1–19 (2017).
44. Beake, B. D., Ogwu, A. A. & Wagner, T. Influence of experimental factors and film thickness on the measured critical load in the nanoscratch test. *Mech. Behav. Micro- Nano-Scale Syst.* **423**, 70–73 (2006).
45. Versaevel, M., Grevesse, T. & Gabriele, S. Spatial coordination between cell and nuclear shape within micropatterned endothelial cells. *Nat. Commun.* **3**, 671 (2012).
46. Hui, C. Y., Jagota, A., Lin, Y. Y. & Kramer, E. J. Constraints on Microcontact Printing Imposed by Stamp Deformation. *Langmuir* **18**, 1394–1407 (2002).
47. Dixon, A. R. *et al.* One-dimensional patterning of cells in silicone wells via compression-induced fracture. *J. Biomed. Mater. Res. A* **102**, 1361–1369 (2014).
48. Nyegaard, S., Christensen, B. & Rasmussen, J. T. An optimized method for accurate quantification of cell migration using human small intestine cells. *Metab. Eng. Commun.* **3**, 76–83 (2016).
49. Murrell, M., Kamm, R. & Matsudaira, P. Tension, Free Space, and Cell Damage in a Microfluidic Wound Healing Assay. *PLOS ONE* **6**, e24283 (2011).
50. McGrath, M. H. & Simon, R. H. Wound Geometry and the Kinetics of Wound Contraction. *Plast. Reconstr. Surg.* **72**, (1983).
51. Cukjati, D., Reberŝek, S., Karba, R. & Miklavĉiĉ, D. Modelling of chronic wound healing dynamics. *Med. Biol. Eng. Comput.* **38**, 339–347 (2000).
52. Du Noüy, P. L. CICATRIZATION OF WOUNDS : II. MATHEMATICAL EXPRESSION OF THE CURVE REPRESENTING CICATRIZATION. *J. Exp. Med.* **24**, 451–460 (1916).
53. Gorin, D. R., Cordts, P. R., LaMorte, W. W. & Menzoian, J. O. The influence of wound geometry on the measurement of wound healing rates in clinical trials. *J. Vasc. Surg.* **23**, 524–528 (1996).
54. Arciero, J. C., Mi, Q., Branca, M., Hackam, D. & Swigon, D. Using a continuum model to predict closure time of gaps in intestinal epithelial cell layers. *Wound Repair Regen. Off. Publ. Wound Heal. Soc. Eur. Tissue Repair Soc.* **21**, 256–265 (2013).
55. Gilman, T. Parameter for measurement of wound closure. *Wounds* **3**, 95–101 (1990).
56. Gilman, T. Wound Outcomes: The Utility of Surface Measures. *Int. J. Low. Extrem. Wounds* **3**, 125–132 (2004).
57. Kiehart, D. P. Wound healing: The power of the purse string. *Curr. Biol.* **9**, R602–R605 (1999).
58. Vedula, S. R. K. *et al.* Mechanics of epithelial closure over non-adherent environments. *Nat. Commun.* **6**, 6111 (2015).

59. Grasso, S., Hernández, J. A. & Chifflet, S. Roles of wound geometry, wound size, and extracellular matrix in the healing response of bovine corneal endothelial cells in culture. *Am. J. Physiol.-Cell Physiol.* **293**, C1327–C1337 (2007).
60. Kam, Y., Guess, C., Estrada, L., Weidow, B. & Quaranta, V. A novel circular invasion assay mimics in vivo invasive behavior of cancer cell lines and distinguishes single-cell motility in vitro. *BMC Cancer* **8**, 198 (2008).
61. Ammann, K. R. *et al.* Collective cell migration of smooth muscle and endothelial cells: impact of injury versus non-injury stimuli. *J. Biol. Eng.* **9**, 19 (2015).
62. Tewary, M. *et al.* A stepwise model of reaction-diffusion and positional information governs self-organized human peri-gastrulation-like patterning. *Development* **144**, 4298 (2017).
63. Ort, C., Lee, W., Kalashnikov, N. & Moraes, C. Disentangling the fibrous microenvironment: designer culture models for improved drug discovery. *Expert Opin. Drug Discov.* 1–13 (2020) doi:10.1080/17460441.2020.1822815.
64. Riahi, R., Yang, Y., Zhang, D. D. & Wong, P. K. Advances in Wound-Healing Assays for Probing Collective Cell Migration. *J. Lab. Autom.* **17**, 59–65 (2012).
65. Hoesli, C. A. *et al.* Dynamics of Endothelial Cell Responses to Laminar Shear Stress on Surfaces Functionalized with Fibronectin-Derived Peptides. *ACS Biomater. Sci. Eng.* **4**, 3779–3791 (2018).
66. Schindelin, J. *et al.* Fiji: an open-source platform for biological-image analysis. *Nat. Methods* **9**, 676–682 (2012).
67. Preibisch, S., Saalfeld, S. & Tomancak, P. Globally optimal stitching of tiled 3D microscopic image acquisitions. *Bioinforma. Oxf. Engl.* **25**, 1463–1465 (2009).
68. Meijering, E., Dzyubachyk, O. & Smal, I. Chapter nine - Methods for Cell and Particle Tracking. in *Methods in Enzymology* (ed. conn, P. M.) vol. 504 183–200 (Academic Press, 2012).

Accessible dynamic micropatterns in monolayer cultures via modified desktop xurography

Raymond Tran[1], Corinne A. Hoesli[1,2]*, Christopher Moraes[1,2,3]*

[1] Department of Chemical Engineering, McGill University, 3610 rue University, Montreal, QC, Canada

[2] Department of Biomedical Engineering, McGill University, 3775 rue University, Montreal, QC, Canada

[3] Rosalind and Morris Goodman Cancer Research Center, McGill University, Montreal, QC, Canada

* co-corresponding authors

E-mail: chris.moraes@mcgill.ca ; corinne.hoesli@mcgill.ca

Supplemental Information

Supplemental Video 1. Wound closure of epithelial monolayer showing distinct lamellipodal behaviour in different wound regions.

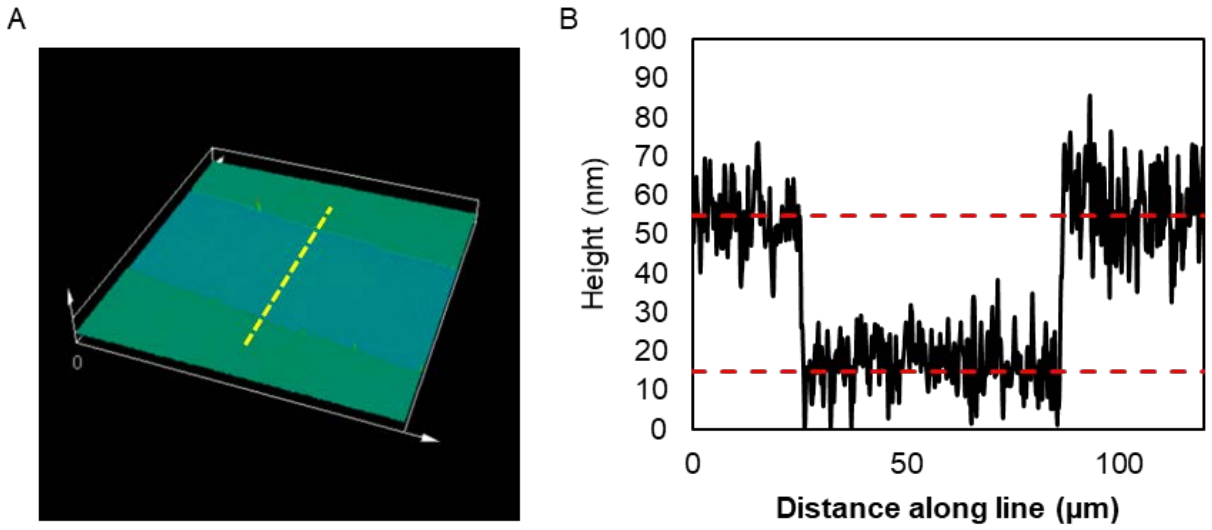

Figure S1: Agarose film layer height is roughly 40 nm thick

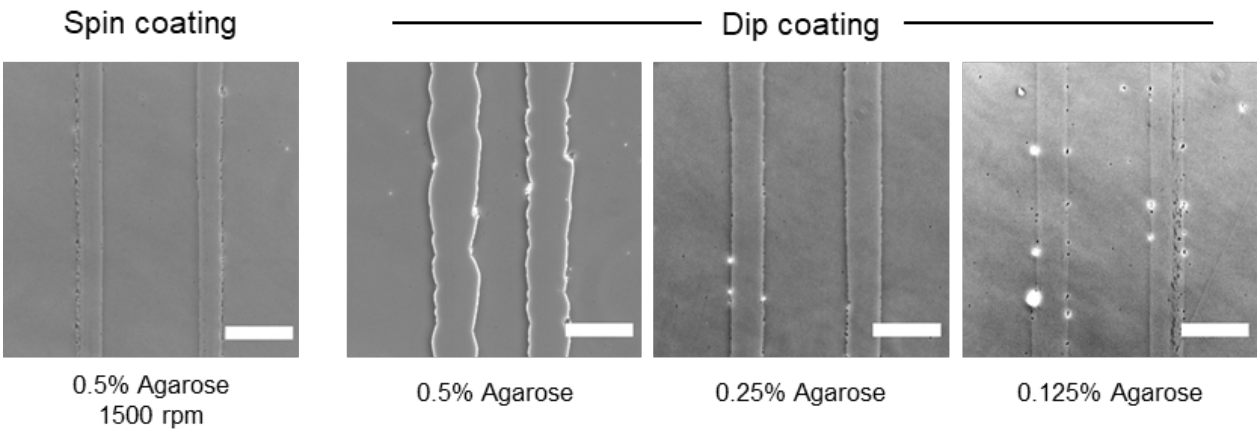

Figure S2: High precision, tear free RMS patterning can also be achieved with a dip coating technique to create agarose film with optimal scribing characteristics. Optimal coating parameters can be determined visually. SuBscribed patterns should have little roughness (<5 µm bumps) and should not have bright outlines when visualized with phase contrast microscopy. Scale bars represent 100 µm.

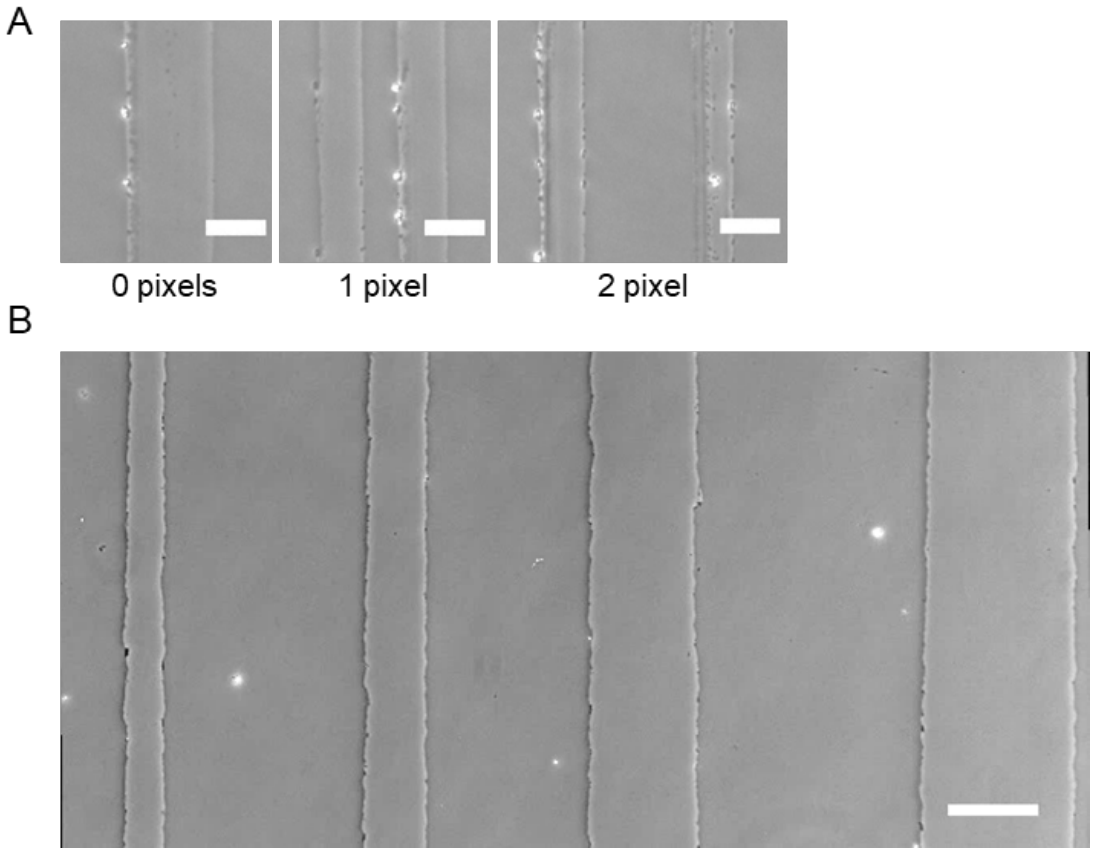

Figure S3: SuBscribing technique allows for precise control of micropattern pitch. (A) High resolution of craft cutter allows for micropattern pitch down to 70 µm. (B) Programming of micropattern design allows for different micropattern dimensions with the same tip. Scale bars: (A) 50 µm, (B) 100 µm.

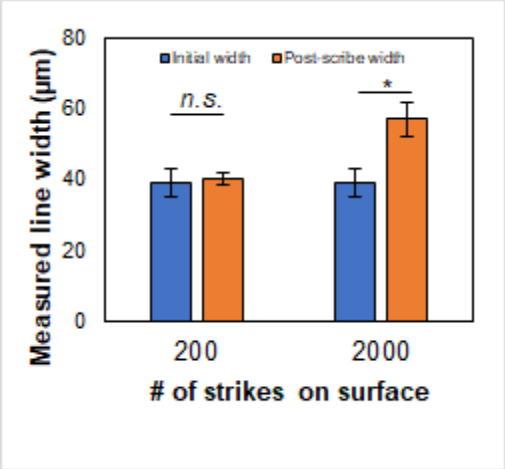

Figure S4: Number of strikes against surface is responsible for tip dulling, not pattern length or geometry. Change in pattern width was characterized by varying the number of impacts for a set scribing length (800 mm). N = 3 needles for each condition, error bars represent standard error on the mean. * represents $p<0.05$ for a Two-way matched ANOVA with Sidak's post-hoc multiple comparisons test.

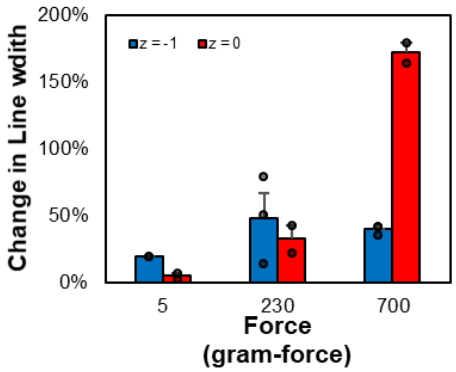

Figure S5: Change in line width can be reduced by lowering the 'force' setting used to scribe micropatterns. Data represents average line width after 2000 scribes at the specified force. Initial line width was 38.6 ± 5.4 µm (n = 15 needles, repeated at least twice for each condition).

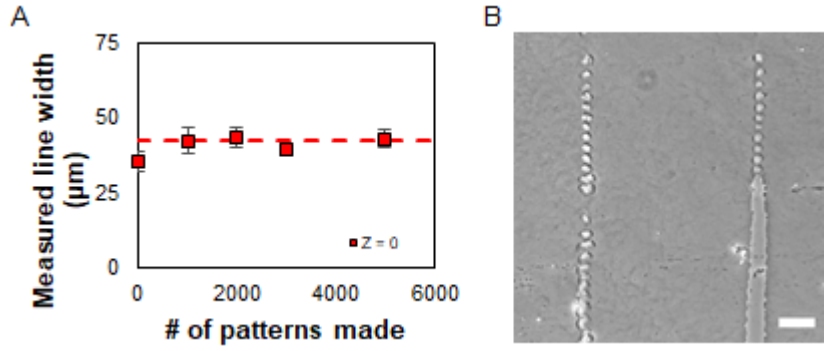

Figure S6: Change in line width can be reduced by calibrating needle tip closer to the glass surface. (A) Measured line width does not significantly change when needle is calibrated at substrate surface. Error bars represent standard deviation of line width. (B) Calibration of the

scribing tip at the surface can lead to the tip missing the surface, resulting in incomplete pattern generation. Incomplete patterns were excluded from analysis. Scale bar represents 50 µm.

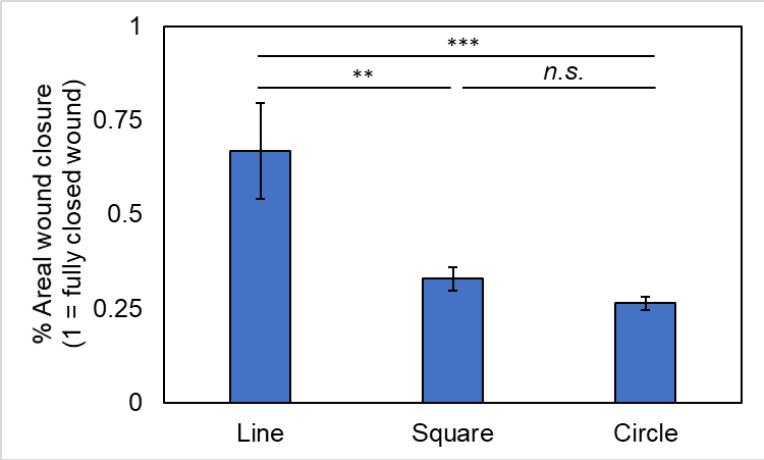

Figure S7: Percent wound closure by area after 1 hour of wounding. ** p<0.01, *** p<0.005 for a one way ANOVA with Tukey post-hoc multiple comparisons test.

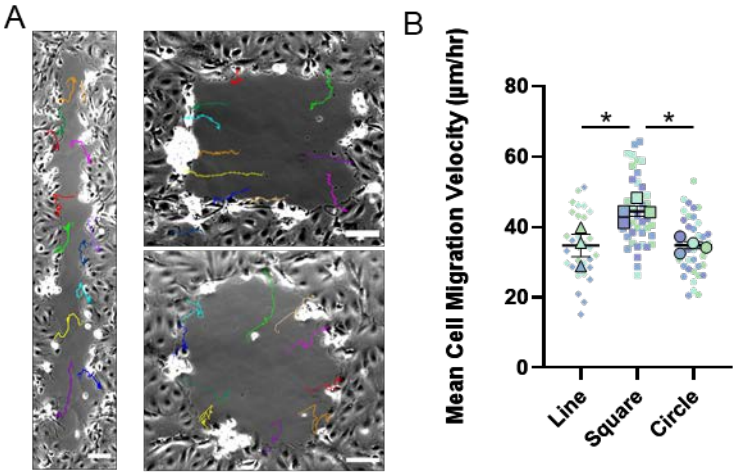

Figure S8: Single cell migration speed reveals cells at wound borders of lines and circles migrate slower than in square geometries. (A) Single cell tracking was performed manually using MTrackJ plugin. (B) Mean cell migration of cells at wound edge for line (n = 3), square (n = 4), and circular (n = 4) wounds. Each data point represents the average migration velocity of 10 cell nuclei at the wound edge. Error bars represent standard error. * p<0.05 for a one way ANOVA with Tukey post-hoc multiple comparisons test. Scale bar represents 100 µm.

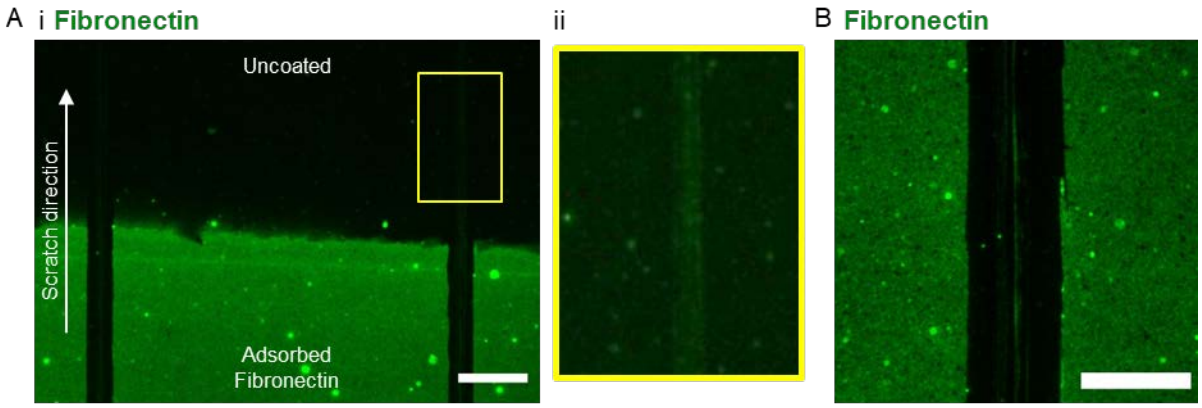

Figure S9: Residual fibronectin is deposited from scratching a fibronectin-coated glass layer. (A) (i) Fibronectin trails are deposited by scratching needle shown by indirect immunostaining of scratched, adsorbed fibronectin. Trails are present in both areas with adsorbed fibronectin and uncoated areas. (ii) Brightness-amplified, magnified image shows fibronectin deposition in uncoated areas. (B) Deposited fibronectin is located at center of scratch pattern as shown by high magnification image. Scale bars: (A) 100 µm, (B) 50 µm.

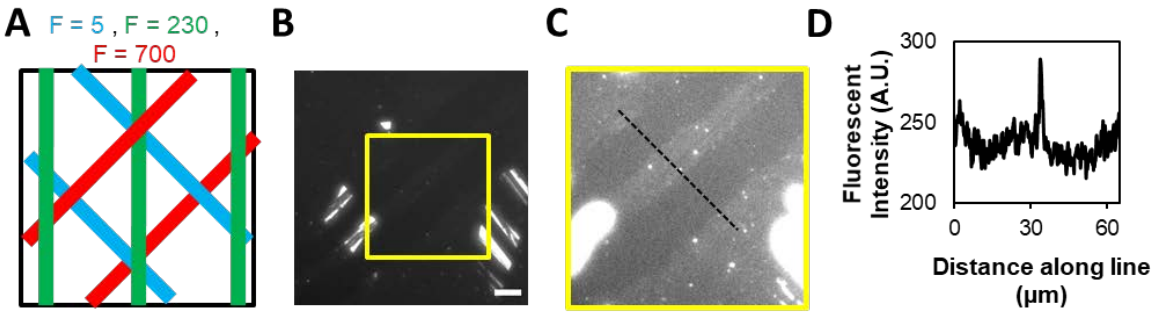

Figure S10: SuBscribing with different force settings can produce varying amounts of fibronectin removal. (A) Map of different scribing forces applied in B and C. (B) Multiple scratch directions were implemented at different forces. (C) Magnified area (yellow box in A) with enhanced brightness and contrast to demonstrate increased fibronectin removal. (D) Fluorescent intensity profile across the dashed black line in C) of adsorbed fibronectin on the surface. Scale bars represent 50 µm.